A combined molecular dynamics simulation and quantum chemical study on the mechanism for activation of the OxyR transcription factor by hydrogen peroxide†

Juraj Kóňa[a,b] and Tore Brinck*[a]

Received 29th March 2006, Accepted 10th July 2006
First published as an Advance Article on the web 8th August 2006
DOI: 10.1039/b604602a

Molecular dynamics (MD) simulations have been performed on the regulatory domain of the *Escherichia coli* OxyR transcription factor for the different chemical states along the mechanistic cycle for its activation by hydrogen peroxide. Conformational analysis indicates that His198 and Arg220 catalytic residues can be involved in the biochemical process of activation of OxyR. On the basis of the simulation data, a detailed mechanism for the oxidation process is suggested in which His198, in the presence of an arginine residue, functions as a unique acid–base catalyst in the successive oxidations of Cys199 and Cys208 by hydrogen peroxide. This mechanistic proposal has been tested by density functional theory (DFT-B3LYP) and *ab initio* (MP2) calculations on model systems. The two oxidations are both identified as nucleophilic substitution reactions of S_N2 type with deprotonated cysteines functioning as nucleophiles. Both reactions have a calculated free energy of activation close to 15 kcal mol^{-1}, which is consistent with the available experimental data on the kinetics of the activation process.

Introduction

Aerobic metabolism generates hydrogen peroxide and organic peroxides as harmful byproducts. Living organisms have evolved a number of defense mechanisms to cope with the resulting oxidative stress, including the OxyR and SoxR transcription factors,[1] specific proteins that interact with prokaryotic promoters. They activate the expression of antioxidant genes in response to hydrogen peroxide and to superoxide-generating compounds, respectively. The mechanistic cycle of activation and deactivation of OxyR of *Escherichia coli* by hydrogen peroxide has been intensively studied using genetic and biochemical methods.[2–7] Zheng *et al.*[3] found by site-directed mutagenesis that Cys199 and Cys208 are absolutely critical for inducible activation by hydrogen peroxide. Mutation of Cys208 results in a protein that shows a constitute low level activity. It was further demonstrated that the activation of OxyR leads to the formation of a disulfide bridge between Cys199 and Cys208 and a mechanism for activation and deactivation of OxyR, which is depicted in Fig. 1, was proposed.[3]

The reduced form of OxyR is oxidized to its active disulfide form by hydrogen peroxide *via* an intermediate of sulfenic acid (OxyR-Cys199-SOH), and subsequently reduced by the enzyme glutaredoxin at the expense of glutathione (Grx + GSH). The formation of the sulfenic acid intermediate has recently been verified by UV–vis spectroscopy on a C208S mutant.[7]

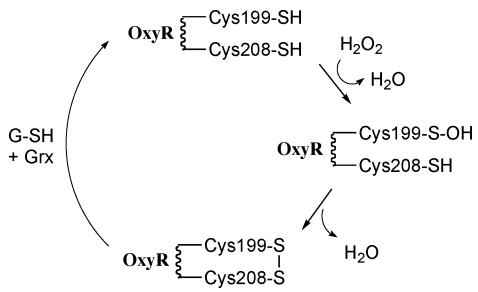

Fig. 1 The redox cycle for the activation of OxyR by hydrogen peroxide proposed by Zheng *et al.*[3]

The proposed redox cycle for the activation and deactivation of OxyR has been questioned by Kim *et al.*[6] They were able to verify the existence of a sulfenic acid intermediate, but found no indication for the formation of an intramolecular disulfide bridge between Cys199 and Cys208. On the basis of these results it was concluded that sulfenic acid is the activated form of OxyR. Furthermore, it was found that in addition to hydrogen peroxide, the protein can be activated by nitroso-compounds and glutathione. The authors suggested that the different activation processes result in different types of transcriptional responses. However, the recent mass spectrometry analyses and *in vivo* labeling assays by Lee *et al.*[7] have confirmed that oxidation of OxyR results in the formation of a specific disulfide bond between Cys199 and Cys208 in the wild-type protein. They speculated that the missing disulfide bridge in the study by Kim *et al.*[6] was an effect of the use of air-oxidized OxyR.

The crystal structure of the oxidized form of OxyR also reveals a disulfide bond between Cys199 and Cys208.[5] Furthermore, the crystal structure of the reduced form shows that the reduction of OxyR involves structural changes in the regulatory domain, which results in the spatial separation of the two cysteines by

[a]*Physical Chemistry, Royal Institute of Technology, SE-10044 Stockholm, Sweden. E-mail: tore@physchem.kth.se; Fax: +46-8-7908207*
[b]*Institute of Chemistry, Slovak Academy of Sciences, Dúbravska cesta 9, SK-845 38 Bratislava, Slovak Republic*

† Electronic supplementary information (ESI) available: CYA atom types, charges and added force field parameters, charts and tables with RMSD of MD simulations, tables of total energies including ZPE corrections, thermal corrections to enthalpy and Gibbs free energy as well as Gaussian input files with Cartesian coordinates of all B3LYP geometries are available as supplementary data. See DOI: 10.1039/b604602a

17 Å.[5] It was suggested that these structural changes may be responsible for the different DNA binding of reduced and oxidized OxyR. Work by Åslund *et al.*[4] has shown that the protein can be transformed from the reduced form to the oxidized form both by a change in the potential of the thiol disulfide redox buffer and by activation by hydrogen peroxide. This implies that in order to facilitate the reversible oxidation–reduction process the two cysteines need to find each other from a distance of 17 Å. It should be noted that the crystal structure of the reduced form is indicative of a large conformational flexibility in the redox-active loop consisting of residues 189–225.[5] Lee *et al.*[7] monitored the structural changes upon hydrogen peroxide activation using fluorescence spectroscopy. They concluded that the conformational change is associated with the disulfide bridge formation rather than the formation of the sulfenic acid. On the basis of time-resolved analyses, it was further determined that the OxyR activation consists of more than one chemical step including disulfide bond formation as well as the physical step of conformational change occurring at a rate of 9.7 s^{-1}. The apparent second order rate constant at low hydrogen peroxide concentrations was determined to be 1.1 10^5 M^{-1} s^{-1},[7] in good agreement with the value of $\sim 10^7$ M^{-1} min^{-1} determined by SDS-PAGE analysis.[4] Lee *et al.*[7] came to the conclusion that disulfide bridge formation most likely precedes the conformational change and it is this latter process that proceeds with a rate of 9.7 s^{-1}. The basis for this is that Cys208 has to compete with GSH in the reaction with Cys199-SOH, and that the rate for the GSH reaction at the 5 mM GSH concentration in the cell is expected to be in the order of 10^3 s^{-1}. Thus, the rate of the disulfide bridge formation is likely to be much higher than 9.7 s^{-1}. Lee *et al.*[7] proposes that oxidation of Cys199 into Cys199-SOH leads to a destabilization of the Cys199 side chain, which results into an expulsion of the side chain out of the interdomain pocket. They further speculate that the high flexibility in the 205–216 region should increase the chances of collision between Cys199-SOH and Cys 208 and subsequent disulfide bond formation. After the disulfide bridge is formed the flexible regions reorganize into the OX conformation, which involves a large structural change in the regulatory domain. This structural change induces a rotation of the OxyR monomers relative to each other that is believed to be important for the change in DNA-binding upon activation.[7,8]

From an organic chemistry point of view, the proposed mechanism for the activation of OxyR to its disulfide form presents two reaction steps that can be characterized as analogous nucleophilic substitutions by thiolate ions or thiols at oxygen and sulfur centers, respectively (Eqn. 1,2).

$$R\text{–}S^- + R\text{–}X\text{–}OH \rightarrow R\text{–}X\text{–}S\text{–}R + OH^-;\ X = O, S \qquad (1)$$

$$R\text{–}SH + R\text{–}X\text{–}OH \rightarrow R\text{–}X\text{–}S\text{–}R + H_2O;\ X = O, S \qquad (2)$$

The mechanistic and energetic aspects of such reactions were elucidated for organic systems using experimental[9] and theoretical methods.[10] Among other things, these studies provide important information concerning the preferable ionization state in which the sulfur nucleophiles react. The calculated reactions with thiolate ions proceeded through significantly lower barriers compared to reactions with thiols.[10] Consequently, reactivity of cysteine-containing species in the redox processes could strongly depend on protonation states. Although the sulfhydryl group of a free cysteine has a too high pK_A value to be deprotonated at physiological pH, it has been demonstrated that a cysteine residue may exist in a thiolate state at physiological pH in a protein systems if the local environment has a high positive electrostatic potential.[11] In OxyR the active-site Cys199 is flanked by the two basic residues (His198 and Arg201) that are absolutely conserved in the OxyR homologues. The crystal structure of the reduced form of OxyR also has another basic residue, Arg266, located close to Cys199.[5] Thus, one or more of these basic residues may aid the deprotonation of Cys199, and thereby activate the residue for the reaction with hydrogen peroxide to form the sulfenic acid and water. In a similar manner it can be speculated that Cys208 needs to be deprotonated before it reacts with the sulfenic acid to form the disulfide bond. However, it is not obvious from the crystal structures which basic residues can be expected to support this process.

In this study we have set out to reexamine the biochemical basis for the mechanism proposed by Zheng *et al.*[3] using a combination of molecular dynamics simulations and quantum chemical calculations. We have used molecular dynamics simulations to investigate the conformational flexibility of the active-site cysteines and the basic residues of the redox-active loop of OxyR in the different chemical states along the mechanistic cycle. On the basis of these simulations we have identified the residues that may take an active part in the different reaction steps. This analysis has subsequently been used to build model systems in which the details of the reactions have been studied by quantum chemical calculations.

Computational methods

Molecular dynamics simulations

The oxidized form of the crystal structures[5] of the regulatory domain of the *Escherichia coli* OxyR transcription factor (PDB ID: 1I6A) was used as a starting structure for molecular dynamic (MD) simulations employing the Amber 6 program package.[12] Our calculations were only based on the oxidized structure with proper modifications (see below), since the crystal structure of the reduced form lacks residues 210–215 from the active site and the Cys199 residue is modified to serine.[5]

Standard parameters from the Amber 1998 force field[13] were used in all calculations. Force field parameters, including atomic charges, for the sulfenic acid residue Cys199-SOH (CYA) were estimated by analogy from the cysteine disulfide (CYX) and the serine (SER) residue parameters, and from data obtained by *ab initio* Hartree–Fock calculations[14] [HF/6–31G(d)] using the Gaussian 98 program package.[15] The electrostatic potential fitting algorithm of Merz-Singh-Kollman scheme[16] was used to estimate atomic charges from the HF/6–31G(d) calculations (CYA atom types, charges and added force field parameters are provided in the Electronic Supplementary Information†).

In the simulations the ionization state for most residues was considered to be the natural at physiological pH. The His173 and all Asp, Glu, Lys and Arg residues were simulated in ionic forms. The His198 residue was modelled in both neutral and ionic forms (see below). 10 $Na^{(+)}$ counterions were added to maintain zero total charge of the system.

Different combinations of chemical states were considered for the Cys199 and Cys208 residues, including disulfide bridge (CYX199, CYX208), both residues protonated (CYS199, CYS208), one residue ionized and the other protonated (CYM199, CYS208), and finally Cys199 in the sulfenic acid state together with Cys208 protonated or ionized (CYA199, CYS208 and CYA199, CYM208). In the calculations, where one of the cysteines was ionized, His198 was considered to be protonated (HIP198). In the rest of the calculations His198 was deprotonated as a neutral HIE (the hydrogen atom on the Nε2 nitrogen of the imidazole ring according to the nomenclature of the Amber force field) and HID (the hydrogen atom on the Nδ1 nitrogen of the imidazole ring). Thus, the following five configurations were investigated: **MD_1** (HIE198-CYX199-CYX208), **MD_2** (HIE198-CYS199-CYS208), **MD_3** (HIP198-CYM199-CYS208), **MD_4** (HID198-CYA199-CYS208) and **MD_5** (HIP198-CYA199-CYM208). The protein was solvated by 9710 TIP3P[17] water molecules in a box with the size of 78 × 67 × 62 Å using LEAP[18] program (total number of atoms in the simulated system is *ca.* 32 000). The MD simulations, preceded with initial minimizations (500 steps), were performed at a constant temperature (300 K) and pressure (101 325 kPa) with use of the Berendsen algorithm[19] employing the SANDER module. Periodic boundary conditions were used together with a Particle Mesh Ewald (PME) method for treating long range electrostatics. A time step of 1.0 fs and the SHAKE algorithm[20] to constrain bonds involving hydrogens were used along simulations with a 10 Å nonbonded cutoff and the nonbonded pair list updated every 25 time steps. Coordinates were saved every 2 ps. All five conformations were carried out to 1 ns. Then, the **MD_3** configuration was continued to 4 ns. All of the MD results were analysed using the CARNAL and PTRAJ modules of Amber 6 and the VMD package.[21]

Quantum chemical calculations

Our model systems consisted of methanethiol (model for the Cys199 and Cys208 residues), guanidinium ion (model for the arginine residues), imidazole (model for the His198 residue) and hydrogen peroxide. All DFT calculations were performed by the Gaussian 98 program package.[15] The geometries were completely optimized with the aid of Becke's three-parameter hybrid density functional-HF method with the Lee–Yang–Parr correlation functional (B3LYP)[22] using the 6–31(+S)G(d) basis set (6–31G augmented by polarization functions on all heavy atoms and diffuse functions on sulfur atoms). In addition, single-point calculations with the 6–31+G(d,p) basis set were carried out using the B3LYP and the second-order Møller–Plesset theory (MP2) methods.[23] All stationary points were characterized as minima or transition states by vibrational frequency calculations. Transition states were verified as having one and only one imaginary frequency. In addition, for each transition state intrinsic reaction coordinate (IRC) calculations were performed to confirm that it connects the correct reactant and product minima. Thermodynamic quantities were calculated at 298 K and 101 325 kPa using standard rigid-rotor and harmonic oscillator partition function expressions. Zero-point corrections and thermal corrections to enthalpy and Gibbs free energies were calculated from unscaled frequencies obtained at the same level as the geometry optimizations. Solvent effects (aqueous solution, $\varepsilon = 78.39$) were estimated by single-point calculations using the polarizable continuum self-consistent reaction field model (PCM-SCRF)[24] at the B3LYP/6–31+G(d,p) level specifying characteristics of the cavity by Bondi's atomic radii scaled by a constant of 1.2 for all other atoms but acidic hydrogens and setting the minimum radius of the added spheres to 1.0.[25] The effective local dielectric constant in the enzyme may vary strongly depending on the local environment. A dielectric constant of 78 would be equivalent to a completely solvent exposed site. Thus, by calculating free energy differences both in gas phase ($\varepsilon = 1.0$) and in aqueous solution the two extrema in solvent effects are represented.

Results and discussion

Firstly, we present the results of the MD simulations on the oxidized, reduced and sulfenic acid forms of OxyR. Our MD analysis is focused on the positions of Cys199, Cys208 and the side chains of the basic residues His198, Arg201, Arg220 and Arg266 in the redox-active loop. Then, our proposed mechanism at the molecular level for the redox process started from the reduced to the oxidized disulfide form of OxyR induced by hydrogen peroxide is explained and investigated by the quantum chemical calculations.

MD simulations of OxyR

In the MD simulations on the oxidized form of OxyR that started from the 1I6A crystal structure (**MD_1**), the protein largely maintains the geometric features of the secondary and tertiary structure of the starting crystal structure. The average root-mean-square deviation (RMSD) of the Cα carbons of the backbone between the crystal structure and the solution structure increased to ~1.4 Å during the first 200 ps and then maintained a stable profile until the end of the 1 ns simulation (Fig. 2).

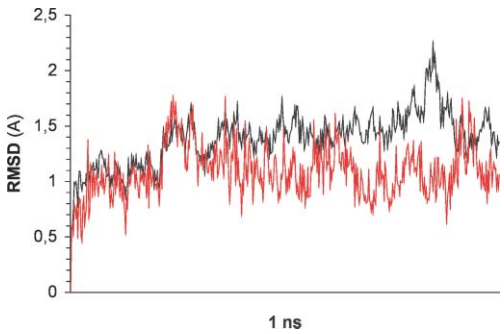

Fig. 2 RMSD (in Å) of the Cα carbons in the oxidized form of OxyR during the 1 ns MD simulation. (Black line—all Cα carbons, red line—Cα carbons of redox-active loop).

The **MD_2** simulation also started from the crystal structure of the oxidized form, but with the disulfide bond broken and the two cysteines both protonated (configuration HIE198-CYS199-CYS208). During the 1 ns simulation the structure maintains the "oxidized" conformation (OX) of the regulatory domain (RMSD of Cα carbons is ~1.6 Å), with the side chains of Cys199 and Cys208 both inside the redox-active loop and located close to each other [d(Cys199-Sγ . . .Sγ-Cys208) ~ 3.9 Å]. Similar results were obtained for a 4 ns MD simulation with ionized Cys199 (**MD_3**, configuration HIP198-CYM199-CYS208) where

the average distance d(Cys199-Sγ...Sγ-Cys208) is 4.6 Å and the RMSD of the Cα carbons is ~1.4 Å. In this case, the redox-active loop exhibited higher mobility compared to other residues of OxyR (the maximum RMSD of the Cα carbons of the redox-active loop is 2.6 Å while it is 1.8 Å for other residues). Both **MD_2** and **MD_3** show that the OX conformation can be stable also when the loop is not restrained by the disulfide bridge. Thus, it can be seen as an indication against the proposal[6] that the OX conformation is not a naturally stable conformation but a result of the crystallization process.

The MD simulations on the Cys199 sulfenic acid intermediate with protonated (**MD_4**, HID198-CYA199-CYS208) and ionized Cys208 (**MD_5**, HIP198-CYA199-CYM208) again indicated the starting OX conformation as the stable one during 1 ns simulations [d(Cys199-Sγ...Sγ-Cys208) ≈4.3 Å and 5.4 Å, respectively]. The redox-active loop with ionized Cys208 showed higher mobility of the loop (maximum RMSD of Cα carbons of the redox-active loop was 2.5 Å in **MD_5** *vs.* 1.8 Å in **MD_4**)

It has been speculated that one or more of the basic residues His198, Arg201 and Arg266 may play important roles in the catalytic process of OxyR.[3,5] The importance of His198 and Arg201 is supported by the fact that these residues are absolutely conserved in the OxyR homologs.[3] In order to determine the functions of the basic residues during the catalytic process, we have analyzed the distances of these residues to the Cys199 and Cys208 residues during the simulations and compiled the results in Tables 1 and 2.

As indicated in Table 1, the side chain of His198 is often found in a position close to the sulfur of Cys199 for all oxidized, reduced and sulfenic acid forms of OxyR (see also Fig. 3). The average d(Cys199-Sγ...Nδ1-His198) and d(Cys199-Sγ...Nε2-His198) range from 5 to 9 Å with minimum distances ~4 Å. The short average distance indicates that His198 could function as

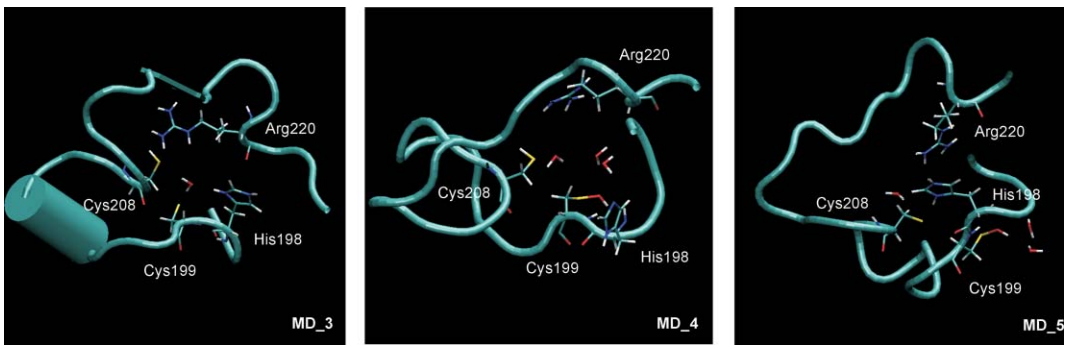

Fig. 3 Snapshots of the redox-active loop of OxyR from **MD_3** (HIP198-CYM199-CYS208), **MD_4** (HID198-CYA199-CYS208) and **MD_5** (HIP198-CYA199-CYM208) simulations which involve positions of Cys199, Cys208, His198 and Arg220 residues and molecules of water found close to the side chains of both redox-active cysteines.

Table 1 Measured distances (in Å) between selected atoms of Cys208 and basic residues (His198, Arg201, Arg220 and Arg266) and the Sγ atom of Cys199 in the redox-active loop of OxyR during 1 ns (**MD_1**, **MD_2**, **MD_4** and **MD_5**) and 4 ns MD simulations (**MD_3**)

Distances/Å	MD_1	MD_2	MD_3	MD_4	MD_5
d(Cys199-Sγ...Sγ-Cys208)					
Average	2.0 ± 0.04	3.9 ± 0.4	4.6 ± 0.7	4.3 ± 0.8	5.4 ± 0.6
Min	1.9	3.2	3.1	3.1	3.1
Max	2.2	5.0	7.3	6.6	7.0
d(Cys199-Sγ...Nδ1-His198)					
Average	5.4 ± 0.4	7.7 ± 0.6	5.6 ± 0.5	7.3 ± 0.8	6.0 ± 0.5
Min	4.4	5.8	4.3	4.9	3.8
Max	6.4	9.0	7.3	8.7	7.1
d(Cys199-Sγ...Nε2-His198)					
Average	7.0 ± 0.3	8.9 ± 0.5	7.5 ± 0.5	6.6 ± 1.0	8.0 ± 0.4
Min	6.1	7.2	5.9	4.1	6.0
Max	7.9	9.8	9.1	8.5	9.0
d(Cys199-Sγ...Cζ-Arg201)					
Average	10.8 ± 0.4	8.9 ± 1.0	11.0 ± 0.4	11.3 ± 0.7	12.0 ± 0.7
Min	9.1	7.3	9.8	9.0	9.5
Max	11.9	11.4	12.6	13.0	13.5
d(Cys199-Sγ...Cζ-Arg220)					
Average	9.5 ± 0.5	9.6 ± 0.7	8.9 ± 1.6	8.4 ± 1.3	10.7 ± 1.0
Min	7.7	7.7	5.5	5.9	8.2
Max	11.6	12.5	13.7	12.2	13.8
d(Cys199-Sγ...Cζ-Arg266)					
Average	11.9 ± 0.6	11.8 ± 0.7	10.8 ± 0.8	10.0 ± 0.5	11.5 ± 0.5
Min	9.6	9.6	9.0	8.5	9.2
Max	13.7	13.2	14.2	11.0	13.1

Table 2 Measured distances (in Å) between selected atoms of basic residues (His198, Arg201, Arg220 and Arg266) in the redox-active loop of OxyR and the Sγ atom of Cys208 during 1 ns (**MD_1**, **MD_2**, **MD_4** and **MD_5**) and 4 ns MD simulations (**MD_3**)

Distances/Å	MD_1	MD_2	MD_3	MD_4	MD_5
d(Cys208-Sγ...Nδ1-His198)					
Average	5.0 ± 0.4	5.2 ± 0.4	5.8 ± 0.6	7.4 ± 1.3	3.0 ± 0.1
Min	3.8	3.7	3.8	5.3	2.7
Max	6.1	6.2	7.7	11.6	3.4
d(Cys208-Sγ...Nε2-His198)					
Average	6.4 ± 0.3	6.5 ± 0.4	7.4 ± 0.6	6.6 ± 1.3	4.9 ± 0.2
Min	5.5	5.4	5.0	4.4	4.4
Max	7.2	7.5	9.5	10.6	5.3
d(Cys208-Sγ...Cζ-Arg201)					
Average	10.7 ± 0.6	9.9 ± 0.9	10.3 ± 0.7	10.0 ± 0.7	9.8 ± 1.0
Min	8.5	8.3	8.9	8.2	7.2
Max	12.0	11.8	12.7	12.4	11.8
d(Cys208-Sγ...Cζ-Arg220)					
Average	9.8 ± 0.6	8.8 ± 0.9	9.2 ± 1.3	7.8 ± 1.3	10.8 ± 1.1
Min	8.0	5.8	5.5	4.8	8.1
Max	11.8	11.7	13.4	12.1	13.9
d(Cys208-Sγ...Cζ-Arg266)					
Average	12.5 ± 0.6	12.0 ± 0.6	13.5 ± 1.0	12.4 ± 1.0	11.1 ± 0.4
Min	10.4	10.6	10.5	10.6	9.8
Max	13.9	13.6	16.5	15.4	12.6

general acid– catalyst, and catalyze the formation of the sulfenic acid intermediate.

We also found that His198 often is located close to Cys208 (Fig. 4) The average *d*(Cys208-Sγ...Nδ1-His198) and *d*(Cys208-Sγ...Nε2-His198) distances range from 3 to 8 Å with minimum distances of ~2.7 Å (Table 2). Thus, His198 is likely to facilitate the deprotonation of Cys208 and possibly also catalyze the formation of the disulfide bridge.

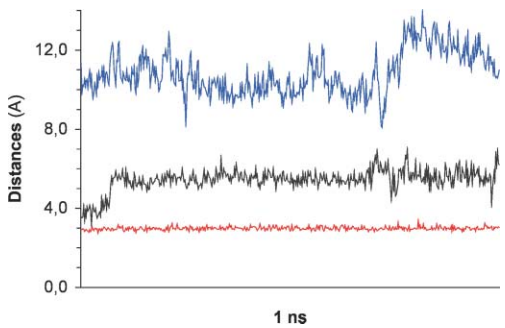

Fig. 4 Distances *d*(Cys199-Sγ...Sγ-Cys208) (black line), *d*(Cys208-Sγ...Nδ1-His198) (red line) and *d*(Cys208-Sγ...Cζ-Arg220) (blue line) in the sulfenic acid form of OxyR with ionized Cys208 (configuration HIP198-CYA199-CYM208) during the 1 ns simulation (**MD_5**).

The analysis of positions of Arg residues indicated that only Arg220 was found close to both cysteines during simulations. It should be noted that in all MD simulations of reduced and sulfenic acid forms of OxyR the redox-active loop was kept in stable OX conformation. Consequently, the positions of Arg201 and Arg266 toward Cys199 or Cys208 were rather different compared with the situation in the crystal structure of the reduced form of OxyR.

On the basis of the MD results, available crystal structures, and the recent study of Lee *et al.*,[7] we propose the following catalytic mechanism at the molecular level for the activation of OxyR (Fig. 5 and 6): in the reduced form of OxyR Cys199 is located in the interdomain pocket flipped out from the redox-active loop which is in the RED conformation. Due to the strong positive electrostatic potential, mainly from Arg266 and Arg201, it is in an ionized state (CYM) as is the neighbor His198 residue (HIP). In contrast Cys208 is completely exposed to the aqueous solution in the crystal structure of the reduced form of OxyR, and therefore fully protonated (CYS) and much less susceptible to attack by hydrogen peroxide. The reactive thiolate ion of Cys199 reacts with hydrogen peroxide to form the sulfenic acid intermediate. In this reaction the positively charged imidazolium moiety of His198 acts as an acid catalyst, which facilitates elimination of the OH^- leaving group from hydrogen peroxide by concomitant proton transfer yielding water and the neutral His198 residue (Cys199-S^- + H_2O_2 + His198-H^+ → Cys199-SOH + H_2O + His198). Our MD simulations do not provide a clear answer to the conformation in which this reaction takes place, since in all MD simulations the redox-active loop of OxyR remained stable in the OX conformation. Lee *et al.* found that the activation of a Cys208S mutant did not result in the change in the fluorescence wavelength that was associated with the formation of the disulfide bond.[7] It was therefore concluded that formation of Cys199-SOH does not lead to a change into the OX conformation. However, considering the distance of 17 Å between the cysteines in the reduced conformation, it seems clear that some conformational changes are necessary to facilitate the reaction between Cys199-SOH and Cys208S. Lee *et al.* propose that oxidation of Cys199 into Cys199-SOH leads to a destabilization of the Cys199 side chain, which results in an expulsion of the side chain out of the interdomain pocket.[7] They further speculate that the high flexibility in the 205–216 region makes it easier for the cysteines to find each other.

Cys208 is first deprotonated by His198 in the presence of Arg220 (Cys208-SH + His198 → Cys208-S^- + His198-H^+). Thereafter the thiolate ion of Cys208 reacts with Cys199-SOH, forming the intramolecular disulfide of OxyR (Cys208-S^- + Cys199-SOH + His198-H^+ → Cys199-S–S-Cys208 + H_2O + His198). Again, the imidazolium moiety of His198 acts as an acid catalyst

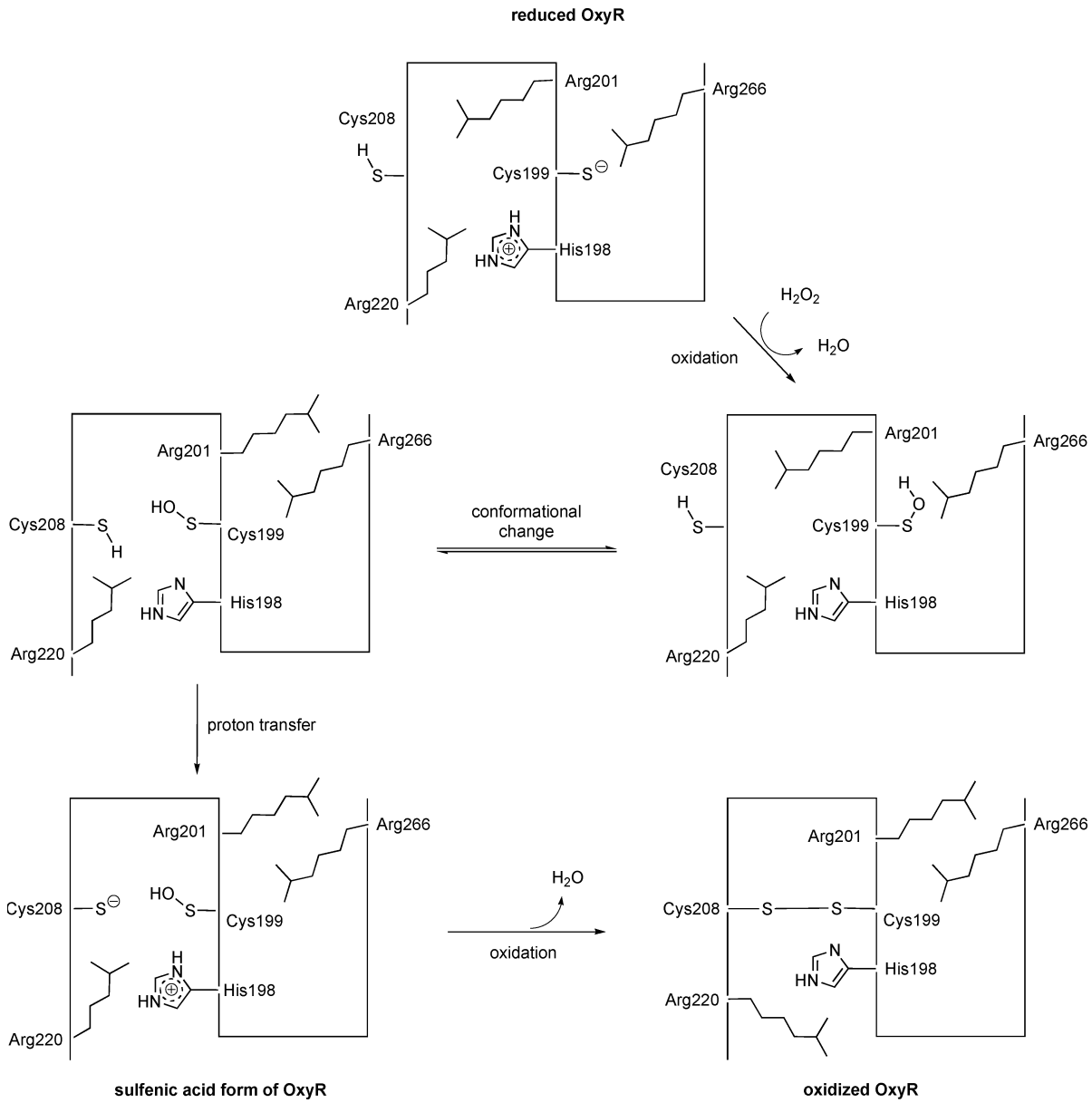

Fig. 5 Proposed mechanism for the activation of OxyR by hydrogen peroxide from the reduced form to the oxidized disulfide form.

facilitating elimination of the OH^- leaving group from the sulfenic acid by concomitant proton transfer, yielding a molecule of water and the neutral His198 residue. The formation of the disulfide bond subsequently induces the transformation into the OX conformation.

DFT calculations on oxidation of OxyR

The above-mentioned redox mechanism of OxyR was tested by quantum chemical calculations and the results are summarized in Table 3 and 4. In the discussion of the results we will refer to energies computed at the B3LYP/6–31+G(d,p) level unless otherwise noted.

Our preliminary semiempirical calculations on the decapeptide sequence of the active-site residues of OxyR (data not shown) as well as the crystal structure indicated possible different roles of the nitrogens (Nδ1 *vs.* Nε2) of the imidazole ring of His198 during the first redox step of OxyR. Complex **1** presents a reaction system, where Cys199 is deprotonated by the Nδ1 nitrogen of His198. The position of the imidazolium ion was built in order to match the conformation and configuration of His198 in reduced OxyR.

The substitution, which starts from **1**, proceeds *via* **2TS** (Fig. 7) and results in complex **3**. According to the DFT calculations the reaction proceeds as an S_N2 bimolecular nucleophilic substitution with concomitant proton transfer. At the transition state the S–O bond has started to be formed and the O–O bond is slightly elongated. The IRC showed that after passing the transition state the proton of the oxygen that forms the bond to sulfur is transferred to the oxygen that leaves as a water molecule. Thereafter the histidine transfers its proton to the oxygen bonded to sulfur. This whole process occurs in one concerted step. During this step the histidine regains its neutral form and can subsequently

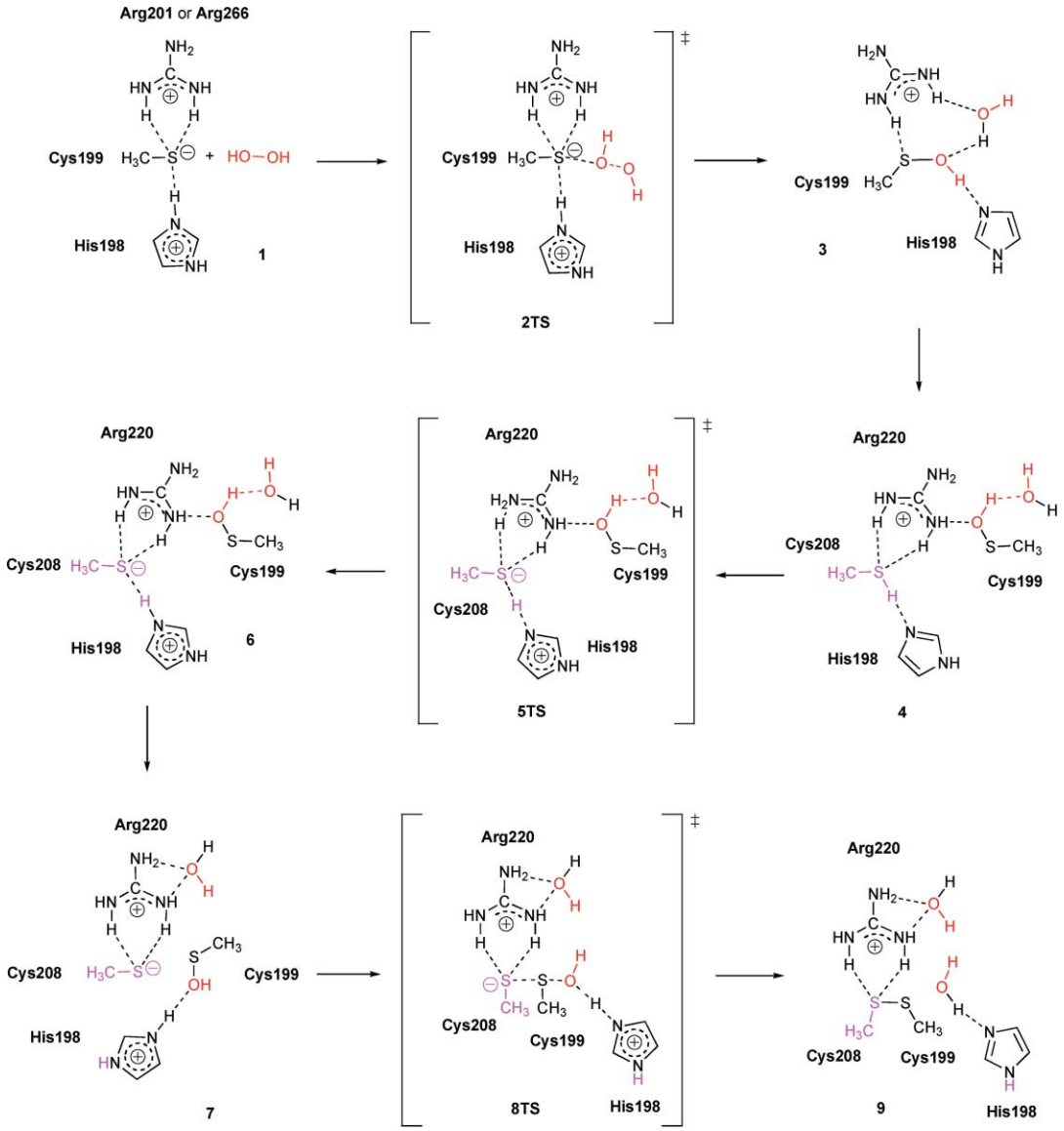

Fig. 6 Computed stationary points along the potential energy surface for the activation of OxyR by hydrogen peroxide. The computations were performed at the B3LYP level using the model systems shown in the figure.

Table 3 Relative energies (ΔE) including ZPE corrections, enthalpies (ΔH) and Gibbs free energies (ΔG) for the first redox step (reaction of Cys199 with hydrogen peroxide) in the gas phase and aqueous solution (ΔG_{sol}) in kcal mol^{-1}

	ΔE^a B3LYP	ΔE^b MP2	$\Delta H_g{}^a$ B3LYP	$\Delta G_g{}^a$ B3LYP	$\Delta G_{sol}{}^c$ B3LYP
1	0.0	0.0	0.0	0.0	0.0
2TS	14.9	14.6	15.1	15.9	14.1
3	−61.1	−70.3	−56.4	−57.7	−58.4

[a] B3LYP/6–31+G(d,p)//B3LYP/6–31(+S)G(d). [b] MP2/6–31+G(d,p)//B3LYP/6–31(+S)G(d). [c] PCM-B3LYP/6–31+G(d,p)//B3LYP/6–31(+S)G(d).

act as an acid–base catalyst in the forthcoming deprotonation of Cys208 and substitution between Cys199-SOH and Cys208.

This reaction has an activation energy at 0 K of 14.9 kcal mol^{-1} at the B3LYP level. The inclusion of thermal and entropy corrections leads to a gas phase free energy of activation of 15.9 kcal mol^{-1} (Fig. 8). Inclusion of solvent effects corresponding to aqueous solution lowers the free energy of activation to 14.1 kcal mol^{-1}. The value for the reaction in the protein is expected to lie in between these values but much closer to the aqueous value, since a lowering of the dielectric constant from 78 to 4, which is a commonly used dielectric constant for proteins, only raises the solution activation free energy by 0.4 kcal mol^{-1} to 14.5 kcal mol^{-1}. Independent of the solvation correction the sulfenic acid formation is found to be strongly exergonic by almost 60 kcal mol^{-1}.

Table 4 Relative energies (ΔE) including ZPE corrections, enthalpies (ΔH) and Gibbs free energies (ΔG) for the proton-transfer reaction (deprotonation of Cys208 by His198) and the second redox step (reaction of Cys199-SOH with Cys208) in the gas phase and aqueous solution (ΔG_{sol}) in kcal mol^{-1}

	ΔE^aB3LYP	ΔE^b MP2	$\Delta H_g{}^a$ B3LYP	$\Delta G_g{}^a$ B3LYP	$\Delta G_{sol}{}^c$ B3LYP
4	0.0	0.0	0.0	0.0	0.0
5TS	1.0	2.2	1.1	2.4	−0.6
6	2.9	4.6	2.8	3.4	0.0
7	3.7	6.0	3.8	6.0	2.0
8TS	14.6	16.2	14.5	19.9	14.6
9	−14.2	−13.9	−9.3	−9.4	−19.2

[a] B3LYP/6–31+G(d,p)//B3LYP/6–31(+S)G(d). [b] MP2/6–31+G(d,p)//B3LYP/6–31(+S)G(d). [c] PCM-B3LYP/6–31+G(d,p)//B3LYP/6–31(+S)G(d).

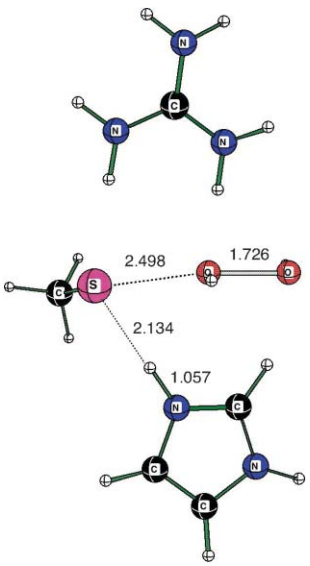

Fig. 7 The B3LYP optimized transition state **2TS** of the first redox step between Cys199 and hydrogen peroxide. Bond lengths are in Å.

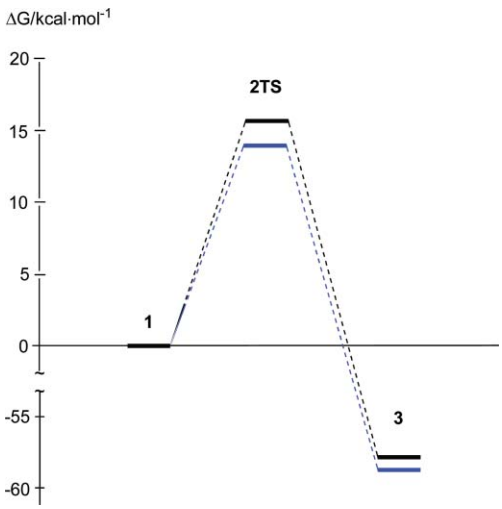

Fig. 8 Gibbs free energy (ΔG) profile for the first redox step between Cys199 and hydrogen peroxide in the gas phase (black line) and aqueous solution (blue line) in kcal mol^{-1}.

It should be noted that we also investigated an alternative transition state for the sulfenic acid formation. In this case the reaction step starts from a complex where the histidine Nδ1 proton is hydrogen bonded to the hydrogen peroxide rather than to Cys 199. This complex can be generated by a conformational interconversion from complex **1**. This reaction sequence can also be characterized as an S_N2 bimolecular nucleophilic substitution with concomitant proton transfer. The gas phase free energy of activation was found to be 2.5 kcal mol^{-1} higher than for the reaction sequence **1**–**2TS**–**3**, but after solvation correction the two activation energies were almost identical. Thus, it is not possible to rule out this alternative reaction sequence from energy considerations. However, we have chosen to focus on the first reaction mechanism for clarity reasons.

The sulfenic acid intermediate formed in the first step of the catalytic reaction reacts further to form the oxidized form of the protein, *i.e.* a disulfide bridge is formed between Cys199 and Cys208. In our calculations this reaction sequence starts from complex **4**. It should be noted that it is not meaningful to compare the energies of complex **3** with **4**, since the protein has to undergo a conformational change that brings the two cysteines in closer proximity to initiate this reaction step. The first reaction step involves a deprotonation of Cys208 by His198 to activate the cysteine for the nucleophilic substitution (**4** → **5TS** → **6**). This proton-transfer reaction has a low activation free energy of 2.4 kcal mol^{-1} ($\Delta G^{\ddagger}$). The resulting complex **6** is 1.0 kcal mol^{-1} higher in energy than the transition state after correction for zero point effects (Fig. 9). It is not unusual that zero point correction leads to a transition state that is lower in energy than the reactant or product if the potential energy surface is very flat along the reaction coordinate, and this effect can be seen as a consequence of the Born–Oppenheimer approximation.[26] The overall free energy change of going from **4** to **6** is 3.4 kcal mol^{-1} in the gas phase and 0.0 kcal mol^{-1} after solvation correction. Complex **6** undergoes a slightly endergonic conformational change into **7** before the final reaction step takes place. This step, the nucleophilic substitution of methanesulfenic acid by methanethiolate ion, proceeds by a bimolecular S_N2 mechanism with concomitant proton transfer from a nitrogen of the imidazolium ion onto the oxygen of the $OH^{(-)}$ leaving group. In this case the proton-transfer lags significantly behind the substitution (Fig. 10). The activation free energies are 13.9 and 12.6 kcal mol^{-1} in gas phase and aqueous solution, respectively. The corresponding effective barriers for the process going from **4** to **9** are 19.9 and 14.6 kcal mol^{-1} (Fig. 9). The best estimate for the protein reaction probably lies in between these two values, but closer to the aqueous value. It should be noted that the MP2 level overall gives similar energy

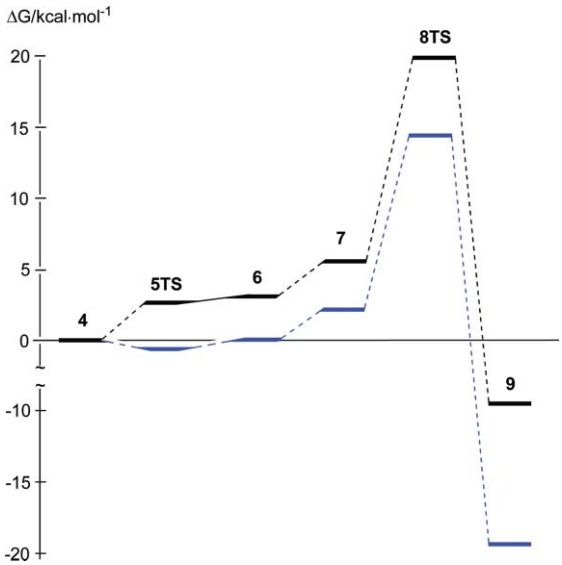

Fig. 9 Gibbs free energy (ΔG) profile for the acid–base reaction between Cys208 and His198 and for the second redox step between Cys199-S-OH and Cys208 in the gas phase (black line) and aqueous solution (blue line) in kcal mol^{-1}.

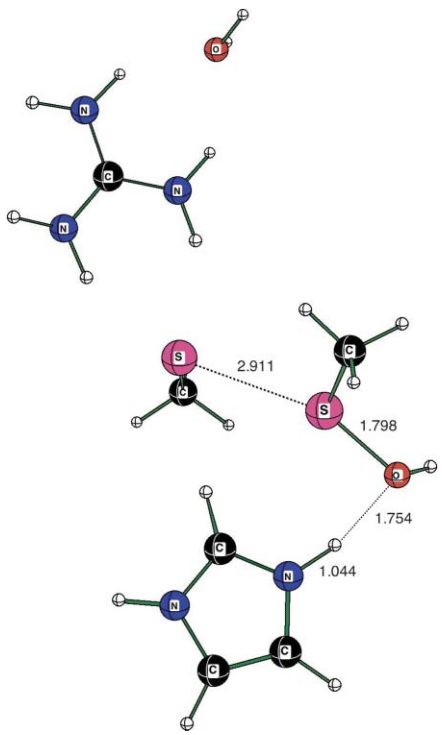

Fig. 10 The B3LYP optimized transition state **8TS** of the second redox step between Cys199-S-OH and Cys208. Bond lengths are in Å.

differences as B3LYP, and thus confirms the validity of the B3LYP results.

Our model system calculations give very similar activation free energies for the two reaction steps, the sulfenic acid formation and the disulfide bond formation, and it is not possible from these results to determine which step is rate-determining. The energy difference is much smaller than the expected effects due to the truncation of the reaction systems. One easily observable consequence of the truncation is that particularly the arginine binds too strongly to the cysteines and/or the substrate. This is of course an effect of the lack of alternative groups in the model systems for the arginine to interact with. In the MD simulations we found the arginines to be highly mobile and to interact more weakly with the cysteines. We tried to investigate what effect this weaker interaction would have on the reaction energetics and found that it seemed to lower the activation energy for both the investigated reaction steps (data not shown). Thus, the interactions with the arginines only need to be sufficiently strong to keep the relevant cysteines deprotonated. This would suggest that our computed activation energies are more likely overestimated compared to ones in *in vivo* systems. The experimental rate of hydrogen peroxide activation is 9.7 s^{-1}, which corresponds to an activation free energy of 16 kcal mol^{-1}. However, Lee *et al.* have suggested that this rate corresponds to the conformational change into the OX conformation and that the actual step of disulfide bond formation has to have a rate that is two to three orders of magnitude higher to compete with the reaction between Cys199-OH and GSH.[7] This corresponds to an activation free energy of 12–13 kcal mol^{-1}, which is in reasonable agreement with our best estimate of around 15 kcal mol^{-1}.

Summary and conclusions

It is noteworthy that the MD simulations of the reduced form of OxyR started from the oxidized crystal structure but with the disulfide bridge broken resulted in no conformational change and kept the cysteines close in space during the 4 ns simulation. This indicates that the OX conformation is a stable protein conformation and not an artefact of the crystallization procedure as has been suggested by Kim *et al.*[6] The significance of the OX conformation was further demonstrated by the simulations on the sulfenic acid intermediate. Although our simulation results do not support the existence of the RED conformation of OxyR, they cannot be interpreted as contradictory to the crystal structure determinations.[5] The time-resolved fluorescence studies by Lee *et al.*[7] demonstrated that the rate of the conformational change is in the order of 10 s $^{-1}$, and thus it cannot be expected that simulations on the nanosecond scale will provide much information on the nature of the conformational change. However, our calculations show that the flexibility of the redox-active loop is significantly greater when one of the cysteines is deprotonated, and that deprotonation thus may induce conformational changes.

Earlier theoretical studies had indicated that the two catalyzed reaction steps, the sulfenic acid formation and the disulfide formation, both require one of the cysteines to be in an ionized state to obtain activation barriers of realistic magnitude.[10] On the basis of the MD simulations we were able to identify residues that can aid the deprotonation and also catalyze the different reaction steps. The His198 residue was found to often attain positions close to Cys199 in the simulations that were relevant for the deprotonation of Cys199 and the sulfenic acid formation. Furthermore, in the simulations relevant for the disulfide bridge formation it was also often found close to Cys208. These, two observations indicate that His198 can function as a general

acid–base catalyst throughout the catalytic cycle and facilitate the deprotonation of both Cys 199 and Cys208.

On the basis of available crystal structures of OxyR and the results of the MD simulations, a model of the catalytic reaction going from the reduced to the oxidized state of the protein has been proposed and tested by quantum chemical calculations in model systems. The reaction starts with Cys199 and Cys208 in ionized and protonated forms, respectively. The first reaction step, the sulfenic acid formation, proceeds by a S_N2 mechanism. During this step His198 regains its neutral form by donating a proton to the leaving group OH^-, which thereby leaves as H_2O. The computed free energy of activation ranges between 14 and 16 kcal mol^{-1}, depending upon the degree of solvation correction.

The formation of Cys119-OH is expected to lead to the expulsion of the Cys199 side chain out of the interdomain pocket and result in a flexible loop around Cys199.[7] This together with the high flexibility of Cys208 is likely to increase the chance of a collision between Cys199-OH and Cys208. The quantum chemical calculations indicate that the disulfide bond formation is preceded by a deprotonation of Cys208 by His198 in the presence of Arg220. This proton transfer has a very low barrier and proceeds with almost no change in free energy. The disulfide bond is formed from the reaction of Cys208 with the Cys199 sulfenic acid. This reaction step, like the sulfenic acid formation, proceeds by a S_N2 mechanism with concomitant proton transfer and His198 functioning as a acid–base catalyst. However, there is a larger solvent effect here, and the computed activation free energy decreases from 19.9 kcal mol^{-1} to 14.6 kcal mol^{-1} when going from gas phase to aqueous solution. After the disulfide bond is formed the protein is believed to undergo a larger conformational change into the OX conformation.[7]

Both the sulfenic acid formation and the disulfide bridge formation are estimated to have an activation free energy in the order of 15 kcal mol^{-1}. This is slightly lower than the 16 kcal mol^{-1} that can be estimated from the experimental rate of activation of 9.7 s^{-1}. However, the rate-limiting step of the activation process is believed to be the conformational change to the OX conformation. Thus, both the sulfenic acid and the disulfide bond formation are expected to be faster processes. It is clear that the size of the model systems somewhat limits the accuracy of the computed reaction energetics. However, there is no reason to believe that a larger and more complete model system would lead to significantly larger activation energies. We can therefore conclude that our MD simulations as well as our quantum chemical calculations support the previously established model for activation of OxyR.[3–5,7] In addition, this study has provided new insight into the dynamics and atomic details of this process.

Acknowledgements

This work was supported by computing resources from the Swedish National Allocations Committee (SNAC). Financial support by the Carl Tryggers foundation (CTS) in the form of a postdoctoral fellowship to JK is gratefully acknowledged. We thank Dr. Fredrik Åslund for helpful discussions and for suggesting this study.

References

1 P. J. Pomposiello and B. Demple, *Trends Biotechnol.*, 2001, **19**, 109–114; G. Georgiou, *Cell*, 2002, **111**, 607–610; J. D. Helmann, *Science's STKE*, 2002, http://www.stke.org/cgi/content/full/sigtrans;2002/157/pe46; D. Barford, *Curr. Opin. Struct. Biol.*, 2004, **14**, 679.
2 I. Kullik, M. B. Toledano, L. A. Tartaglia and G. Storz, *J. Bacteriol.*, 1995, **177**, 1275–1284.
3 M. Zheng, F. Åslund and G. Storz, *Science*, 1998, **279**, 1718–1721.
4 F. Åslund, M. Zheng, J. Beckwith and G. Storz, *Proc. Natl. Acad. Sci. U. S. A.*, 1999, **96**, 6161–6165; K. Tao, *FEBS Lett.*, 1999, **457**, 90.
5 H. Choi, S. Kim, P. Mukhopadhyay, S. Cho, J. Woo, G. Storz and S. Ryu, *Cell*, 2001, **105**, 103–113.
6 S. O. Kim, K. Merchant, R. Nudelman, W. F. Beyer, Jr., T. Keng, J. DeAngelo, A. Hausladen and J. S. Stamler, *Cell*, 2002, **109**, 383–396.
7 C. Lee, S. M. Lee, P. Mukhopadhyay, S. J. Kim, S. C. Lee, W. S. Ahn, M. H. Yu, G. Storz and S. E. Ryu, *Nat. Struct. Mol. Biol.*, 2004, **11**, 1179–1185.
8 J. Zaim and A. M. Kierzek, *Nucleic Acids Res.*, 2003, **31**, 1444–1454.
9 G. M. Whitesides, J. E. Lilburn and R. P. Szajewski, *J. Org. Chem.*, 1977, **42**, 332–338; R. P. Szajewski and G. M. Whitesides, *J. Am. Chem. Soc.*, 1980, **102**, 2011–2026; G. M. Whitesides, J. Houk and M. A. K. Patterson, *J. Org. Chem.*, 1983, **48**, 112–115; R. Singh and G. M. Whitesides, *J. Am. Chem. Soc.*, 1990, **112**, 1190–1197; R. Singh and G. M. Whitesides, *J. Am. Chem. Soc.*, 1990, **112**, 6304–6309.
10 S. M. Bachrach, J. M. Hayes, T. Dao and J. L. Mynar, *Theor. Chem. Acc.*, 2002, **107**, 266–271; J. M. Hayes and S. M. Bachrach, *J. Phys. Chem. A*, 2003, **107**, 7952–7961; S. M. Bachrach, D. W. Demoin, M. Luk and J. V. Miller, Jr., *J. Phys. Chem. A*, 2004, **108**, 4040–4046; Z. Benková, J. Kóňa, G. Gann and W. M. F. Fabian, *Int. J. Quantum Chem.*, 2002, **90**, 555–565; B. Cardey and M. Enescu, *ChemPhysChem*, 2005, **6**, 1175–1180.
11 C. Sun, M. J. Berardi and J. H. Bushweller, *J. Mol. Biol.*, 1998, **280**, 687–701; A. Gustafsson, P. L. Pettersson, L. Grehn, P. Jemth and B. Mannervik, *Biochemistry*, 2001, **40**, 15835–15845; A. Claiborne, J. I. Yeh, T. C. Mallett, J. Luba, E. J. Crane, III, V. Charrier and D. Parsonage, *Biochemistry*, 1999, **38**, 15407–15416.
12 D. A. Case, D. A. Pearlman, J. W. Caldwell, T. E. Cheatham, III, W. S. Ross, C. L. Simmerling, T. A. Darden, K. M. Merz, R. V. Stanton, A. L. Cheng, J. J. Vincent, M. Crowley, V. Tsui, R. J. Radmer, Y. Duan, J. Pitera, I. Massova, G. L. Seibel, U. C. Singh, P. K. Weiner and P. A. Kollman, *AMBER 6*, University of California, San Francisco, 1999.
13 T. E. Chetham, III, P. Cieplak and P. A. Kollman, *J. Biomol. Struct. Dyn.*, 1999, **16**, 845–861.
14 C. C. J. Roothan, *Rev. Mod. Phys.*, 1951, **23**, 69.
15 M. J. Frisch, G. W. Trucks, H. B. Schlegel, G. E. Scuseria, M. A. Robb, J. R. Cheeseman, V. G. Zakrzewski, J. A. Montgomery, R. E. Stratmann, J. C. Burant, S. Dapprich, J. M. Millam, A. D. Daniels, K. N. Kudin, M. C. Strain, O. Farkas, J. Tomasi, V. Barone, M. Cossi, R. Cammi, B. Mennucci, C. Pomelli, C. Adamo, S. Clifford, J. Ochterski, G. A. Petersson, P. Y. Ayala, Q. Cui, K. Morokuma, D. K. Malick, A. D. Rabuck, K. Raghavachari, J. B. Foresman, J. Cioslowski, J. V. Ortiz, B. B. Stefanov, G. Liu, A. Liashenko, P. Piskorz, I. Komaromi, R. Gomperts, R. L. Martin, D. J. Fox, T. Keith, M. A. Al-Laham, C. Y. Peng, A. Nanayakkara, C. Gonzalez, M. Challacombe, P. M. W. Gill, B. G. Johnson, W. Chen, M. W. Wong, J. L. Andres, M. Head-Gordon, E. S. Replogle and J. A. Pople, *Gaussian 98, Revision A.7*, Gaussian, Inc., Pittsburgh, PA, 1998.
16 B. H. Besler, K. M. Merz, Jr. and P. A. Kollman, *J. Comput. Chem.*, 1990, **11**, 431–439; U. C. Singh and P. A. Kollman, *J. Comput. Chem.*, 1984, **5**, 129–145.
17 W. L. Jorgensen, J. Chandrasekhar, J. D. Madura, R. W. Impey and M. L. Klein, *J. Chem. Phys.*, 1983, **79**, 926–935.
18 C. E. A. F. Schafmeister, W. S. Ross and V. Romanovski, *LEAP*, University of California, San Francisco, 1995.
19 H. J. C. Berendsen, J. P. M. Potsma, W. F. van Gunsteren, A. D. DiNola and J. R. Haak, *J. Chem. Phys.*, 1984, **81**, 3684–3690.
20 J. P. Ryckaert, G. Ciccotti and H. J. C. Berendsen, *J. Comput. Phys.*, 1977, **23**, 327–341.

21 W. Humphrey, A. Dalke and K. Schulten, *J. Mol. Graphics*, 1996, **14**, 33–38.
22 A. D. Becke, *J. Chem. Phys.*, 1993, **98**, 5648–5652; C. Lee, W. Yang and R. G. Parr, *Phys. Rev. B: Condens. Matter*, 1988, **37**, 785–789; B. Miehlich, A. Savin, H. Stoll and H. Preuss, *Chem. Phys. Lett.*, 1989, **157**, 200–206.
23 C. Møller and M. S. Plesset, *Phys. Rev.*, 1934, **46**, 618; M. Head-Gordon, J. A. Pople and M. J. Frisch, *Chem. Phys. Lett.*, 1988, **153**, 503–506; M. J. Frisch, M. Head-Gordon and J. A. Pople, *Chem. Phys. Lett.*, 1990, **166**, 275–280; M. J. Frisch, M. Head-Gordon and J. A. Pople, *Chem. Phys. Lett.*, 1990, **166**, 281–289.
24 S. Miertuš, E. Scrocco and J. Tomasi, *Chem. Phys.*, 1981, **55**, 117–129; S. Miertuš and J. Tomasi, *Chem. Phys.*, 1982, **65**, 239–245; M. Cossi, V. Barone, R. Cammi and J. Tomasi, *Chem. Phys. Lett.*, 1996, **255**, 327–335.
25 T. Brinck, A. G. Larsen, K. M. Madsen and K. Daasbjerg, *J. Phys. Chem. B*, 2000, **104**, 9887–9893.
26 F. Jensen, in *Introduction to computational chemistry*, John Wiley & Sons, Chichester, 1999, pp. 3, 56.

